Wearable disposable electrotherapy

Mohamad FallahRad [1] ✉, Kyle Donnery [1], Mojtaba Belali Koochesfahani[1], Zeeshan Chaudhry[2], Rayyan Bhuiyan[1], Benjamin Babaev[1], Matthew Saw[1], Tiffany Liu[1], Miguel R. Diaz Uraga [1], Mahdi Zaman[1], Kisholoy Saha[1], Osvaldo Velarde[1], Ayman Rddad[1], Niranjan Khadka [1], Myesha Thahsin[1], Alexander Couzis [2] & Marom Bikson[1]

We design and validate an electrotherapy platform without electronic components, using printed, abundant, environmentally benign materials. Whereas existing electrotherapy devices use an independent power source and electronics to generate and control stimulation currents, our design eliminates the need for these components. Device production relies only on scalable additive manufacturing and common materials, minimizing cost and environmental impact. The disposable single-use platform (as discreet as adhesive bandages) is activated simply by placement on the body. A prescribed electrotherapy dose is regulated by a flexible 3D electrochemical architecture tailored to each application by a bespoke operational theory. The single-dose usability of this platform is a categorical shift from existing approaches with durable equipment that require programming and assembly to disposable electrodes for each use. Our Wearable Disposable Electrotherapy technology can be distributed like pharmacotherapy, with indications spanning neuromodulation of brain disorders, skin health and wound healing, transcutaneous drug delivery, and bioelectronic medicine.

Applications of non-invasive electrical stimulation span treatment of pain and headache[1,2] depression, addiction, age-related cognitive decline[3,4] wound healing[5,6] aesthetic uses[7], bioelectronic medicine, and drug delivery[8]. Electrical therapy devices have become compoundingly complex (microelectronics, stretchable electronics, wireless connectivity, etc.)[6,9,10]. Battery-powered electronic devices must be connected to electrodes before each use, attached to the body, a discharge program initiated, and charged for subsequent use. The form factor of conventional devices is thus a barrier to adoption of electrotherapy in healthcare and compliance. The up-front-cost and cumbersomeness of conventional electrical therapy contrasts with the "take and forget" usability of capsule pharmaceuticals - which contributes to the significant differences in pharmaceutical- vs electrotherapy-based healthcare[11].

In this paper, we report on the first electrotherapy platform that provides auto-initiated (upon application to the skin) controlled discharge in a single-use, disposable, low-cost, conformable patch. Enabling these features is an integrated printable design, absent of any electronics (no circuit components), with power source, self-limiting mechanism, and interface elements made from environmentally benign common materials assembled layer by layer. The entire platform is thus printed on a common substrate, with an emergent 3D electrochemical architecture. In human trials, we establish our printed battery technology, with self-limited electrical output to prescribed doses, with "apply and forget" usability. The dematerialized product is economically- and environmentally-efficient compared to electronics-based equipment.

The Wearable Disposable Electrotherapy platform supports scalability and distribution models akin to pharmaceuticals. Each therapy-strip can be discreetly carried, applied in any environment, and disposed after use, similar to an adhesive bandage. Indeed, one application is accelerated wound healing. Adoption is seamless as caregivers (e.g., nurses, parents) are provided a product operationally identical to adhesive bandages. The addition of drugs allows active transdermal delivery[12]. Almost any existing application of non-invasive electrotherapy can be emulated, enhancing access to neuromodulation for pain (migraine) and neuropsychiatric disorders[3,13].

[1]Department of Biomedical Engineering, The City College of New York, New York, NY, USA. [2]Department of Chemical Engineering, The City College of New York, New York, NY, USA. ✉e-mail: Fallahrad.mohamad@gmail.com

We show the creation of Wearable Disposable Electrotherapy involved the development of system design processes, a theoretical framework for self-limited dose control, battery cell technology, and battery pack architecture adapted to scalable manufacturing processes. For an exemplary device, in exhaustive detail, each design element is verified, and performance is validated in human trials. We additionally demonstrate the platform's effectiveness for three applications: neuromodulation, accelerated wound healing, and iontophoresis. The impact of usability, economics, environmental, and healthcare equity is explained.

Results
System features
Our goal is to develop a single-use disposable electrotherapy device that can compete in cost and usability with pharmaceuticals. The

design of the Wearable Disposable Electrotherapy platform addresses interdependent constraints spanning automatically initiated and controlled dosing, power density, packaging, and scalable manufacturing with only common, environmentally benign, and nonhazardous materials. The device design supports broad application-specific flexibility (dose, placement) (Fig. 1a).

1. The central innovation of this platform is the avoidance of conventional electronics (e.g., printed circuits, heavy metals), which hinder an environmentally responsible single-use device. The therapeutic dose is controlled through a printed structure using modular battery cells with interconnects. Together, the 3D battery pack structure, cell shape, tailoring areal energy density to thickness, active materials, and mass inventory provide the requisite voltage and dose control. Dose ramping is achieved through power-load interface design (internal battery pack
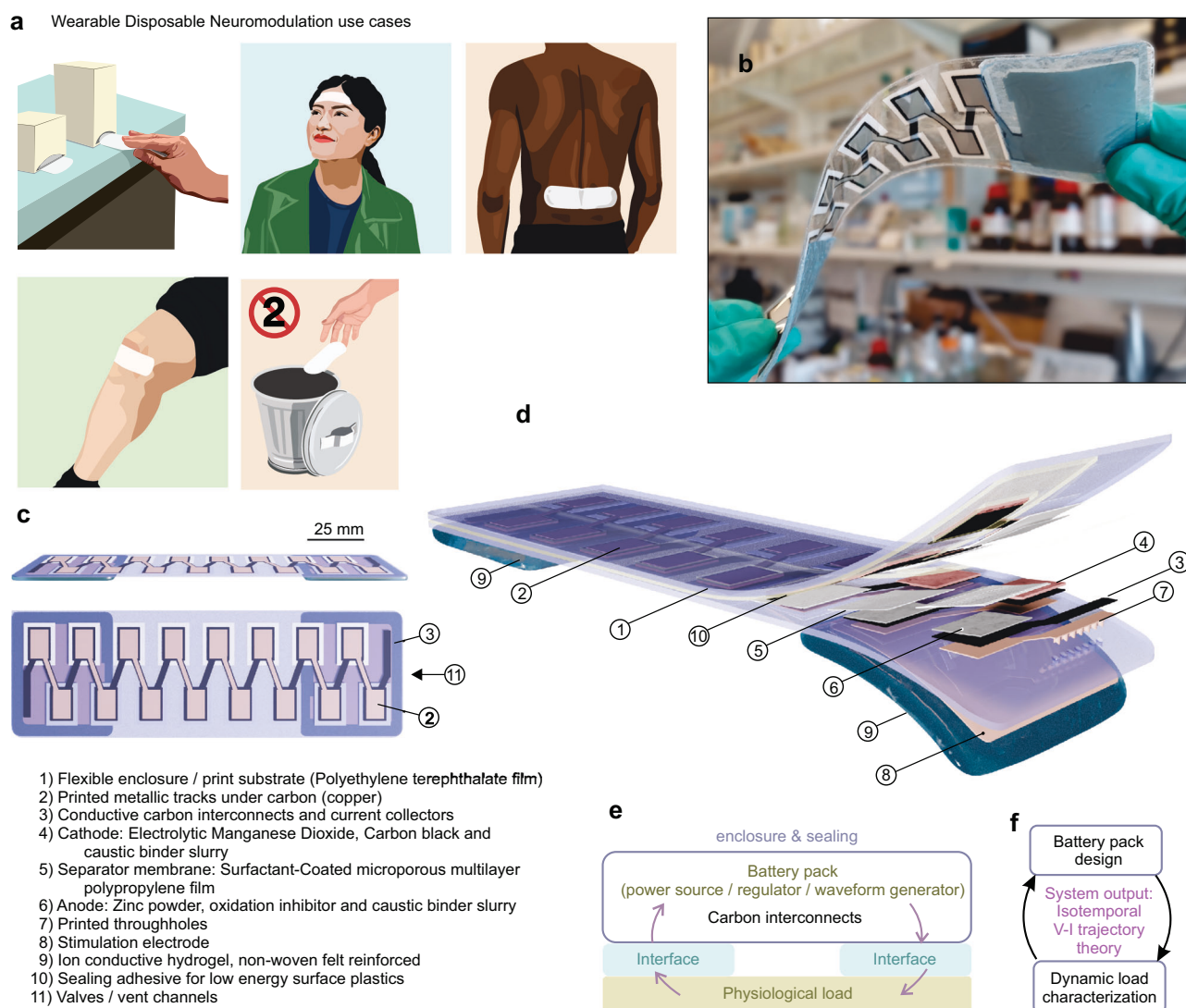
a Wearable Disposable Neuromodulation use cases

b

c

d

1) Flexible enclosure / print substrate (Polyethylene terephthalate film)
2) Printed metallic tracks under carbon (copper)
3) Conductive carbon interconnects and current collectors
4) Cathode: Electrolytic Manganese Dioxide, Carbon black and caustic binder slurry
5) Separator membrane: Surfactant-Coated microporous multilayer polypropylene film
6) Anode: Zinc powder, oxidation inhibitor and caustic binder slurry
7) Printed throughholes
8) Stimulation electrode
9) Ion conductive hydrogel, non-woven felt reinforced
10) Sealing adhesive for low energy surface plastics
11) Valves / vent channels

e

f

Fig. 1 | Wearable Disposable Electrotherapy Device. a Application-specific single-use devices are distributed and used akin to disposable bandages or pharmaceuticals. Applications include brain/cranial nerve stimulation (e.g., cognition, headache), electrical stimulation for pain, and accelerated wound healing. Devices are disposable as they are made without conventional electronics, using environmentally benign materials. **b** Photograph of exemplary device. **c, d** Device performance is enabled by a layered geometry of active materials and interfaces (element types 1-11) printed onto a common substrate (which becomes the device enclosure).

e System diagram: The battery pack discharge is initiated and governed by interaction, through the interface, with the target physiological load. Application-specific therapeutic dose (e.g., neuromodulation, transdermal drug delivery, wound healing bandage) is thus controlled by the device shape and battery pack design. **f** Unlike prior neuromodulation or battery technologies, discharge is neither current nor voltage controlled. Rather, device chemistry and architecture (battery packs) are designed based on a bespoke discharge theory.
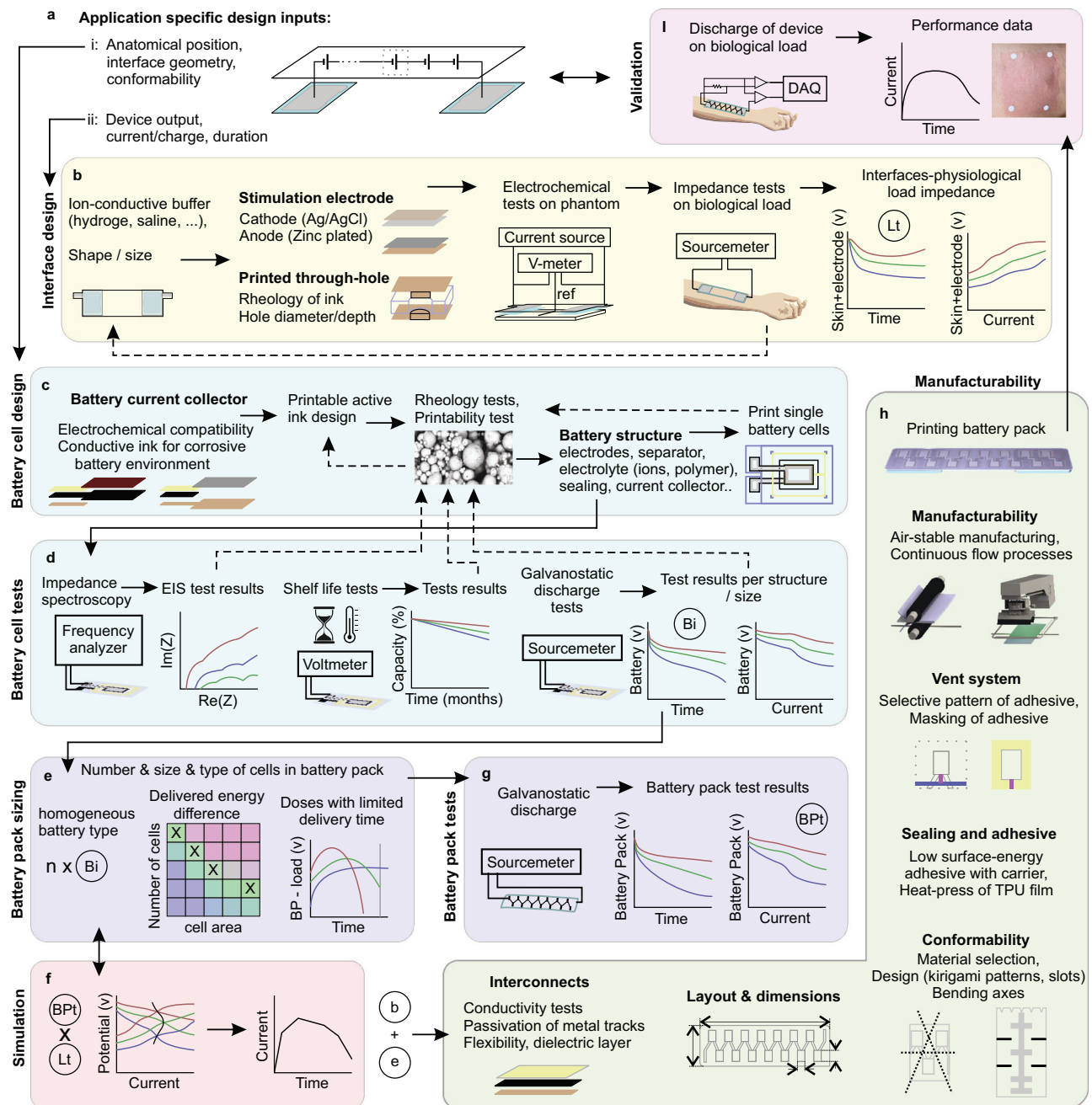
Fig. 2 | Design pipeline enabling Wearable Disposable Electrotherapy. A comprehensive workflow supports design and validation of devices. **a** Application-specific design inputs. **b** Interface design including and load characterization. **c** Battery cell design (chemistry and structure). **d** Battery cell characterization and tests. **e** Battery pack sizing (cell types, size, number). **f** Performance simulation using Isotemporal Trajectory Theory. **g** Battery pack tests. **h** Design for conformability and manufacturability. **i** Design validation in human trials. Design stages (colored regions, dashed arrow: within stage testing) incorporate design input and produce design outputs (solid arrows/circled letters) for other stages. In practice, the system design of Wearable Disposable Electrotherapy is iterative between stages.

resistance, electrodes, hydrogel thickness, and ion mobility) based on the progressive impedance changes associated with device application/removal.

2. The common (embedded) substrate for all power/interface components removes any steps by the user ("no assembly required"). Devices are activated upon contact, where the body completes the device discharge circuit (Fig. 1e). Therefore, to use the device, one needs only to apply it (e.g., absence of any controls, even a start button).

3. The platform's 3D architecture is manufactured entirely using additive/subtractive fabrication with common/benign materials,

including active materials based on alkaline Zn/MnO_2 electrochemistry. Moreover, the battery does not require charging; it is fully activated during fabrication.

4. Packing, power (maximum current, capacity), shape, and conformability design requirements are addressed in an iterative design workflow (Fig. 2). There is an overlay of electrochemical design, working-temperature regulation (Supplementary Fig. 1), mechanical design to support needed conformability, and sealing structures (including venting system; Supplementary Fig. 2d, Supplementary Fig. 3c, Supplementary Fig. 3f).

5. Control of discharge is unlike all prior electrotherapy or battery technology, where electronics are required to regulate output. To design an electrochemical self-limited output to a prescribed dose, we developed the Isotemporal-Trajectory theory (detailed in Supplementary Notes 1).

As a consequence of these features, Wearable Disposable Electrotherapy devices may be distributed and used as economically and simply as pharmaceuticals. Our overall approach is to dematerialize the design and simplify the user experience of wearables. This contrasts with the general trend for increasingly complex wearable electronics[9,14,15].

System design
Achieving these features involved the innovation of an integrated product development pipeline (Fig. 2). Engineering and testing processes are divided into stages with design outputs that become the inputs (solid arrows) to subsequent design modules. Each stage is explained below and then demonstrated/validated in detail for an exemplary platform and three electrotherapy applications.

Replication of efficacy of a stimulation device by Wearable Disposable Electrotherapy requires only the imitation of dose[16], namely relevant electrical output over time (Fig. 2aii) and electrode interface shape/position (Fig. 2ai). For each application, dose is therefore the primary design input (Fig. 2a) against which device elements (design output) are verified/validated.

Interface design (Fig. 2b) includes stimulation electrodes (anode/cathode) and an ion-conductive buffer (e.g., hydrogel sheet). Interface element's electrochemical capacity[17,18] is tested, the design refined accordingly (e.g., printing vs. electrochemical corrosion vs. electroplating), leading to load-impedance characterization using galvanostatic stimuli: current intensities straddle the application-specific operating range with a given compliance voltage limit. This selected voltage affects the performance of the final prototype, including current ramp-up time and peak, and number of cells in the battery pack. Note the load includes device interfaces (stimulation electrodes) and the physiological load.

Battery cell design is an iterative process involving architecture, anode/cathode inks, current collectors, separator membrane, and electrolyte (Fig. 2c). Varied battery cell designs and sizes are prototyped and verified (Fig. 2d; galvanostatic discharge using current levels match those used for load impedance tests, shelf life, EIS).

If a single battery does not have sufficient potential for delivering targeted dose, a battery pack consisting of a series of batteries is required (Fig. 2d; Supplementary Fig. 4c). Battery pack design considers the required energy, self-limiting mechanism, and voltage (matched to the compliance voltage from load impedance tests). Battery pack sizing (Fig. 2e) includes selection of the number of battery cells, cell types, and size of cells. Battery packs may be homogenous - with a single battery cell type/size - or inhomogeneous - with distinct battery types controlling specific aspects of dose. Sized battery packs are fabricated and galvanostatically verified (Fig. 2g).

For dose control, unlike prior electrotherapy devices with electronic output control, our platform's fundamental challenge is the nonlinearity of both the energy source (battery pack) and the load. As part of the battery pack sizing stage, we developed a design theory (Fig. 2f). Data from galvanostatic testing of the load impedance across subjects and of varied battery pack designs are parameters to simulate the discharge of the coupled system. The governing equation (Supplementary Notes 1) of Isotemporal-Trajectory theory is:

$$V_B(I_n, t \,|\, \alpha_B, e_B) = V_L(I_n, t \,|\, \alpha_L, e_L) \qquad (1)$$

Where the voltages V_B and V_L are the independently characterized battery pack and load subsystems, respectively; I_n are constant current stimuli; α_B and α_L are internal parameters of each system; and e_B and e_L

are environmental factors. Varied battery pack performance is simulated and selected designs are passed to subsequent design-for-manufacturing and human trial stages.

Given application-specific battery pack and interface element designs, the associated manufacturing processes are developed (Fig. 2h; Supplementary Notes 2). These processes include interconnect design, sealing techniques, venting systems, and conformable design. The additive manufacturing process must assemble these elements (device 3D architecture) concurrently - while also being scalable, economical, and environmentally benign. Final prototypes are tested against design inputs in human trials (Fig. 2i) to validate each application of Wearable Disposable Electrotherapy.

Device structure
Wearable Disposable Electrotherapy device elements (Fig. 1c, d) include application-specific electrochemical cells connected in series[19] (Supplementary Fig. 4c), internal interconnects and external interface elements (stimulation electrodes and ion conductive buffer), sealing, venting systems and skin adhesive/dressing based on application.

Printed battery cells consisting of an anode and cathode, with corresponding cell terminals, are sealed to prevent electrolyte losses as well as to eliminate cell-to-cell parasitic losses that result from electrolyte sharing between cells (Supplementary Fig. 2). The anode terminal of the first cell and the cathode terminal of the last cell are the terminals of the battery pack (power source; Supplementary Fig. 4c). These terminals are connected to the interfaces, consisting of the stimulation electrode and ion-conductive buffer, which in turn provide connectivity to the body (Fig. 1e).

The batteries adapt primary aqueous alkaline Zinc/Manganese Dioxide chemistry. Electrolytic Manganese Dioxide (EMD) is the cathode active material and metallic zinc is the active anode material (Supplementary Fig. 5). This chemistry offers safety and high energy density[20,21]. The anode and cathode are separated by a specialized membrane made from a porous polypropylene (PP) film laminated to a non-woven PP, coated with a hydrophilic surfactant for aqueous applications. The membrane is suitable for extreme pH levels, and it maintains mechanical stability when wet. High device discharge rate is achieved by this high-porosity membrane, high surface area of each cell, and high conductivity interconnects. As the application is not steady-state (i.e., current changes as a function of time), EIS characterizes the dynamic behavior of varied cell constructs (Supplementary Fig. 5h–j), which in turn informs battery pack design. Hydrogen gas generation (which can deform the enclosure) is minimized using a zinc alloy (with <100 ppm of indium and bismuth), and corrosion inhibitor additive to the alkaline electrolyte and is managed using a vent system (individual battery vents converging to a central 1 mm width channel, Supplementary Fig. 2d, Supplementary Fig. 3c), which also supports effective vacuum sealing.

In order to fit the required number of cells in series within the physical constraints of the device area and for scalable manufacturing, we developed an innovative cell printing and packing approach. Anodes, cathodes, and their connections are printed in successive steps, in a symmetric geometric fashion on a plastic substrate. The interconnects between anodes and cathodes produce the required in-series connection between cells. The substrate that the elements are printed on becomes the enclosure of the device: The substrate is folded along its symmetry axis, aligning each anode element to its corresponding cathode element (of each cell), resulting in a fully functionalized and sealed battery pack (Supplementary Fig. 4a).

The device includes regions of relatively high flexural rigidity (battery cells) bisected by axes of low flexural rigidity (Supplementary Fig. 4bi). This mechanical design, that results from the planar arrangement of battery cells, enhances device conformability. Application specific devices incorporate further design elements for conformability including articulated enclosures pattern cuts, or regions of
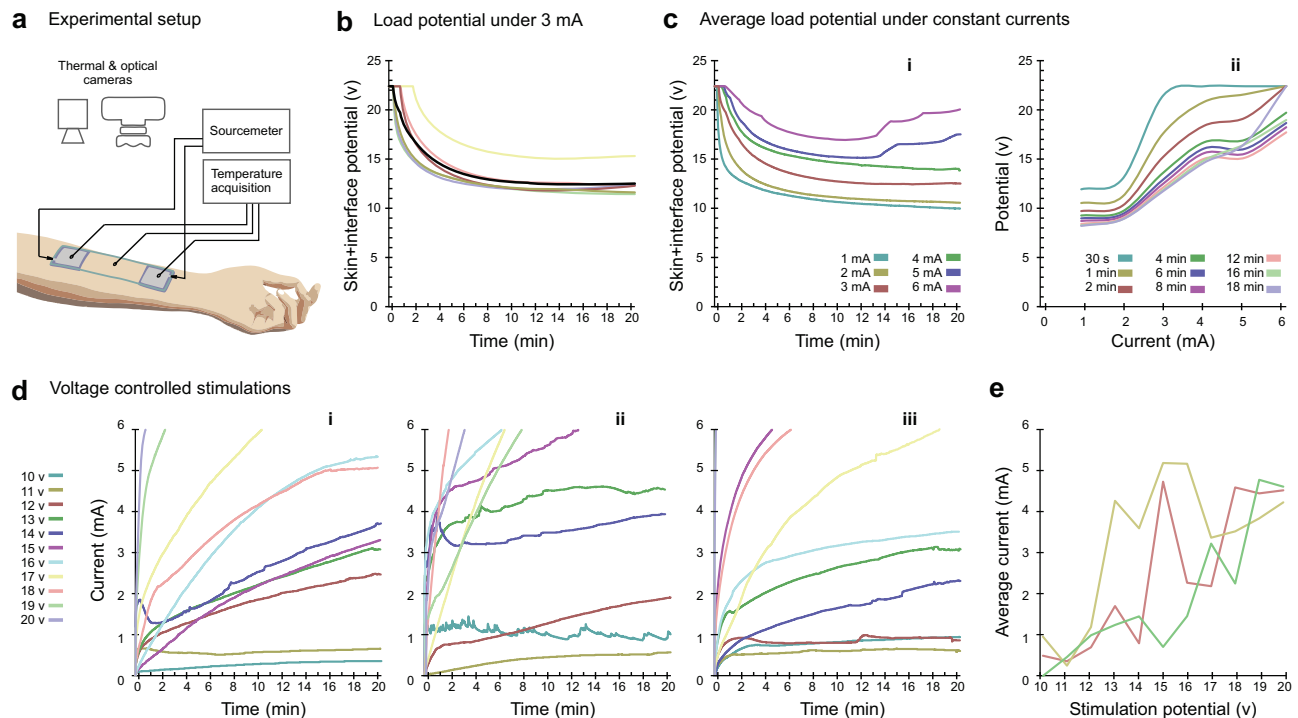
Fig. 3 | Load characterization for exemplary Wearable Disposable Electrotherapy device design. a Experimental setup using the interface test device. **b** Potential of load (skin+interface) under 3 mA over 20 min for individual subjects (colored lines) and average (black line). **c** i: Average load potential over 20 min under constant currents (used to size battery packs), associated ii: isotemporal V-I curves (used to simulate battery pack discharge). **d** Voltage-controlled stimulations over 20 min for three subjects (**i, ii, iii**) **e** average current (over the active duration) for fixed applied voltages. Note unreliable non-monotonic relationship for voltage-controlled stimulation.

low flexural rigidity (e.g., interface regions with a single substrate (Supplementary Fig. 4biv).

The substrate material must support sufficient surface adhesion and compatibility with ink solvents and the extreme pH conditions of battery processes, while also providing the required mechanical characteristics for the application. Polyethylene Terephthalate (PET) is favored for disposability, cost-effectiveness, and environmentally friendly properties, aligning with Wearable Disposable Electrotherapy specifications.

Interconnect tracks are printed on both sides of the substrate; on the inner side (upon folding) connecting sequential batteries and on the outer side connecting battery pack terminals to the electrode of the interface (Supplementary Fig. 2; Supplementary Fig. 3). The track interconnects consist of a narrower copper track beneath a wider conductive carbon track, topped by a broader dielectric layer. This architecture results in interconnects with 75% greater conductivity.

The device is coupled to the skin through the interface elements (hydrogels), which support both electrical charge delivery and adhesion of the device on skin. The interface elements (on the exterior of the substrate) are electrically connected to the battery pack (inside the pack) by throughhole interconnects (Supplementary Fig. 3b): an array of micrometer-sized channels through the substrate filled with metallic ink. Channel size is adjusted to ink rheology.

The battery current collector for the anode is printed copper ink. For the cathode, carbon ink alone or on top of metallic ink is necessary to prevent the corrosion of the current collector. For anode stimulation electrodes, zinc ink, and for cathode stimulation electrodes Ag/AgCl ink printed on a copper surface enhance charge-passing capacity especially for DC applications.

The exemplary Wearable Disposable Electrotherapy device is designed for low-intensity transdermal stimulation applications[7,22] with a target dose of 3 ± 1 mA DC average over 20 min (single-use ~150 mC/cm² capacity) in a conformable packaging with 25 cm² interface electrodes

(12 cm inter-electrode distance). A significant design aspect involves ensuring tolerability by limiting current transients at the initiation ($\tau > 1$ min), end of stimulation (managed in conventional electrotherapy equipment with microcontrollers), and instantaneous peak current not to exceed 5.5 mA. Hydrogel electrodes are designed for reliable current passage (~0.6 mm thick; volume resistivity of ~500 Ω.cm;[23], biocompatibility (ISO 10993-5, ISO 10993-10), and provide mechanical adhesion of the device to the skin (moderate skin pull-off adhesion, 20–50 g/cm; relative high adhesion on the device side, >100 g/cm), with no residue (e.g., felt reinforced) or irritation.

The exemplary Wearable Disposable Electrotherapy device (Fig. 1b–d, Supplementary Fig. 3) comprises of printable layers forming a battery pack (five layers), conductive interconnects (four layers), PET sheets enclosure (two layers), sealant (three layers), PP strips to mask sealant as normally closed valves connecting inner space of batteries to vent channel, and ion-conductive hydrogels. The 3D design results in a varied number of layers depending on position along device plane - from 3 at enclosure ends, to 9 over internal battery cells, to 11 at conductive hydrogels (not including vents and through holes) (Supplementary Fig. 2b and 3c).

Load impedance characterization

Unlike prior electrical stimulation devices that are current-controlled or voltage-controlled, the Wearable Disposable Electrotherapy output is governed by the electrical coupling of two dynamic sub-systems: the battery pack and the load (Fig. 1f). The design of Wearable Disposable Electrotherapy involves galvanostatic characterization of the load impedance - which includes the device interface elements and physiological load (Fig. 2). For this stage, a test device is used composed of only the interface components (stimulation electrodes and ion-conductive buffer), devoid of battery pack material. The test device is powered by a sourcemeter (Fig. 3a) generating fixed current intensities spanning the target electrotherapy dose with a limited

voltage-compliance (reflecting a given battery pack). Because Wearable Disposable Electrotherapy is applied to the body in a pre-energized state, for load impedance testing the sourcemeter is energized prior to the placement of the interface components on the body.

To characterize the load impedance for the exemplary device, interface-components were applied to subjects' forearms connected to sourcemeter providing 1-6 mA current-controlled with a 22.4 V compliance. In separate experiments, we considered the response to constant-voltage stimulation with 10–20 V in 1 V increments (17 total conditions; $n = 10$ subjects).

Under constant 3 mA stimulation, voltage gradually decreased in each subject (Fig. 3b). On average across subjects, voltage decreases gradually under 1–4 mA constant currents, but increases at ~14 min for 5–6 mA current (Fig. 3ci), reflecting controlled electrode capacity design. These relationships are summarized in isotemporal lines (average load, Fig. 3cii; individual subject load, Supplementary Fig. 6) and used for subsequent battery pack design. The load impedance is dynamic as a function of applied current and time, reflecting nonlinear processes at the stimulation electrode[17] and skin[24,25].

Batteries do not provide constant current and their internal voltage/impedance is a nonlinear function of the current drawn; this creates a complex interdependence between energy source and load impedance. In subsequent design steps (Fig. 2), we show how the load impedance data informs battery pack design to produce self-regulated Wearable Disposable Electrotherapy (theory in Supplementary Notes 1).

For contrast, we show constant voltage stimulation (10–20 V) produces unreliable current (Fig. 3d). Current fluctuates on an experiment-wise basis over time. Current is not monotonic with time or applied voltage. These results confirm that voltage-controlled stimulation (i.e., from an idealized battery) is not reliable for (DC) electrotherapy.

Battery pack design

The embedded battery pack powers the physiological load through interfaces and must satisfy all previously defined constraints: mechanical, form factor, manufacturing limits, cell chemistry and construct (ink formulation, screen thickness, separator type, electrolyte composition, etc), given the load's impedance at the prescribed dose current.

The battery pack voltage during a current-controlled discharge (I_{dose}) over the interval $0 < t < T_{dose}$, with similar type and size and total of N cells in the pack can be described as:

$$V_P(I_{dose}, t) = \sum_{i=1}^{N} V_b(I_{dose}, t, size) \qquad (2)$$

where $V_b(I_{dose}, t, size)$ is the voltage of a single battery cell with specific size at time t for a given current-controlled discharge (I_{dose}) (Fig. 4a).

In a homogeneous pack, only the number of cells and cell size are design variables since areal power density is fixed for a given cell construct. To explore this two-dimensional space, candidate cell sizes from a range are characterized at I_{dose}, and total battery pack potential is calculated by multiplication of cell voltage by the number of cells in the pack (Fig. 4bi).

Calculated voltage difference between the battery pack and the load determines the net energy gap. The minimal energy difference, over the targeted dose, between the battery pack and load is given by:

$$\min\left\{ \int_{t=0}^{T_{dose}} (V_{P,N,type}(Idose, t) - V_L(Idose, t)) dt \right\} \qquad (3)$$

From configurations with minimal energy difference (marked combinations in Fig. 4bi), any option that either overshoots early and exhausts prematurely or continues to deliver energy beyond the prescribed dose duration is discarded. The design that satisfies the entire therapeutic window without these shortcomings is ultimately chosen (Fig. 4bii).

If finer control of the delivery profile is required, cell types become an additional design variable and an inhomogeneous pack can be assembled. Mixing flat discharge, cathode limited, limited-power or limited-capacity cells (Supplementary Fig. 5e, f, g) further controls initial transients, sustained current, and tail-end energy delivery. The chosen pack is then prototyped and fully characterized (Fig. 4e). Measured discharge curves feed simulations against the average and recorded impedance distribution, and only after this verification step is the design prototyped for human trials.

For the exemplary device, the selection of battery chemistry and a homogenous pack design reduces the optimization to cell area and number: 1.5 cm² with 14 cells was deemed optimal for the specified target dose. The average potential of single 1.5 cm² cells over a 20 min span across various discharge rats (1-6 mA) was measured ($n = 72$); both average performance (Fig. 4ci, solid line) and performance variation due to variations in battery fabrication (Fig. 4ci, shaded). The average potential of the cells for up to a discharge depth of 1 mAh was calculated (Fig. 4cii). The performance of single battery cells was characterized using EIS and used to develop an associated circuit analog model (Fig. 4d). The lumped-parameter device impedance model reflects electrochemical processes occurring in the cell[26]. These single cell data are then used to inform iterations of battery chemistry (Supplementary Fig. 3h–j) and battery pack design.

Verification and system simulation

For the exemplary target dose and load, having designed the chemistry, size, and number of cells for the battery pack, we manufactured and tested battery packs under galvanostatic discharge ($n = 60$ battery packs). The average potential of battery packs over a 20 min span across various fixed discharge rates (1–6 mA) was measured; both average performance (Fig. 4ei, solid line) and performance variation due to variation in battery fabrication (Fig. 4ei, shaded) is reported. The average potential of the battery packs for up to a discharge depth of 1 mAh was calculated (Fig. 4eii). For this characterization, we extend the testing duration beyond the targeted dose.

The battery pack discharge dynamics is represented in isotemporal lines (colored dashed lines; Fig. 4fi). These are overlaid with isotemporal lines from the load average (colored solid line; Fig. 4fi). For each time point (color), the intersection of these lines is represented (solid black line; Fig 4fi). This is the temporal evolution of the intersections between the voltage-current characteristics of the battery and of the load is the projected device output. According to l isotemporal-trajectory theory (Supplementary Notes 1) this is the simulated Wearable Disposable Electrotherapy. This analysis is repeated across multiple subjects, based on their individual load analysis (Supplementary Fig. 6; Fig 4fii); taken together these output trajectories is the simulated operational envelope of the device. Reflecting successful prior stages of device design: (1) trajectories show the current will initially ramp up with limited decrease in voltage; (2) the current reaches a maximum value within the target range, after which the voltage decreases substantially, limiting current delivery; (3) a further decrease in voltage ramps the current down and concludes the discharge.

Temperature can influence device performance because the cells and interfaces contain polymers. The patch's minimal mass and thickness causes it to equilibrate with skin temperature within a few seconds of application[27] (Supplementary Fig. 1).

Stability (shelf-life) testing of the exemplary Wearable Disposable Electrotherapy pack assessed the battery pack's capacity. Over 15 days, the average voltage decreased by 5.25 mV per cell daily, which,
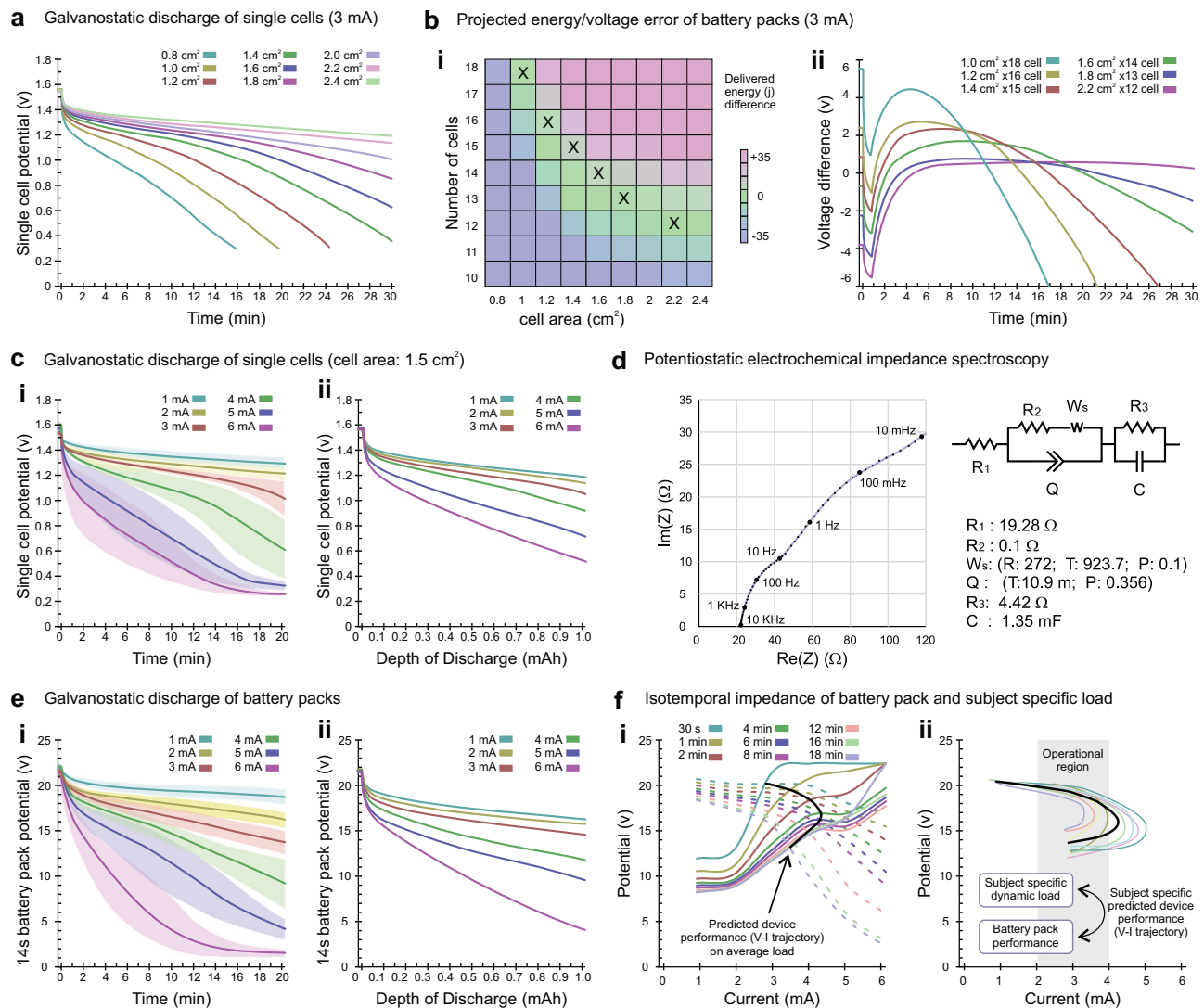
Fig. 4 | Battery cell and pack design (sizing), validation, and stimulation for exemplary Wearable Disposable Electrotherapy. a Galvanostatic discharge curve of single-cell batteries (average) with different cell sizes under 3 mA current over 30 min; **b i**. Projected energy (j) error of battery packs with 10 to 18 cells made from cells with different sizes under 3 mA discharge vs average of energy required to stimulate load with 3 mA during 20 min (x: selected designs for next stage); **b ii** Voltage difference between six battery pack designs (selected based on minimal projected energy error) and voltage of load over 30 min at 3 mA. **c** Galvanostatic discharge curve of single cells with sized area of 1.5 cm² (solid line: mean, shaded:

SD); **d** Potentiostatic electrochemical impedance spectroscopy of single cell per 1 cm² area over frequency range of 10 mHz to 10 kHz with bias equal to OCV of freshly assembled battery and fitted model; **e** Galvanostatic discharge curve of sized (14 cell, 1.5 cm² area) battery pack, **i**: over 20 min time (solid line: mean, shaded: SD), **ii**: over-discharge depth; **f i** Isotemporal V-I curve of sized battery pack discharge (dashed lines) with overlaid average isotemporal V-I load curve (solid line). The intersection of these lines is the predicted discharge for the sized device into the average load (black line). **f ii** Given each subject's V-I load curve, a subject-specific (colored lines) and average (black line) sized device discharge is simulated.

allowing for a ~20% decrease (e.g., from 1.55 V to 1.2 V per cell), indicates a stability of 66.7 days (i.e., over two months of stability at the prototype stage).

Validation

With chemistry and sizing designed for the exemplary application, the exemplary Wearable Disposable Electrotherapy discharge performance was validated ($n = 10$ subjects; Fig. 5a). Devices satisfied all other requirements, with a final thickness of 1.25 ± 0.07 mm and weight of 10.5 ± 0.1 g. Devices were applied to the skin (t = 0) for 20 min, and the generated voltage (Fig. 5b) and current (Fig. 5c) measured. Across subjects, voltage gradually decreased while current gradually increased ($\tau = 8.7 \pm 3.4$ min) to a target (3.6 ± 0.8 mA) where current was sustained. A further decrease in voltage reduced current. Stimulation was sustained for the 20-minute application with average current dose per subject range of 2.1–4.0 mA, within

specification for all subjects (average voltage 15.4 ± 2.4 V; average current 2.8 ± 0.7 mA; average power 41.8 ± 12 mW). As the device was removed, the current was progressively ramped down and eventually aborted ($\tau = 5.0 \pm 0.5$ s).

Voltage-current trajectories (Fig. 5d) exemplify Wearable Disposable Electrotherapy dose control and performance along system-design simulations (compare with Fig. 4fii). Discharge is neither strictly current-controlled nor voltage-controlled, but current passing for each subject is governed by the battery pack design and the dynamic impedance response (Supplementary Notes 1). Load impedance initially decreased with current application (Fig. 5e) but reliably plateaued and normalized across subjects (range 4–7 kΩ at 18 min). Isotemporal trajectory theory predicted individual dosing (Supplementary Fig. 6c) with an accuracy of 0.22 ± 0.08 mA (within 7.2% of 3.5 mA).

Discomfort during electrotherapy was assessed by conventional VAS rating[23] at 11 time points during stimulation. Stimulation was well
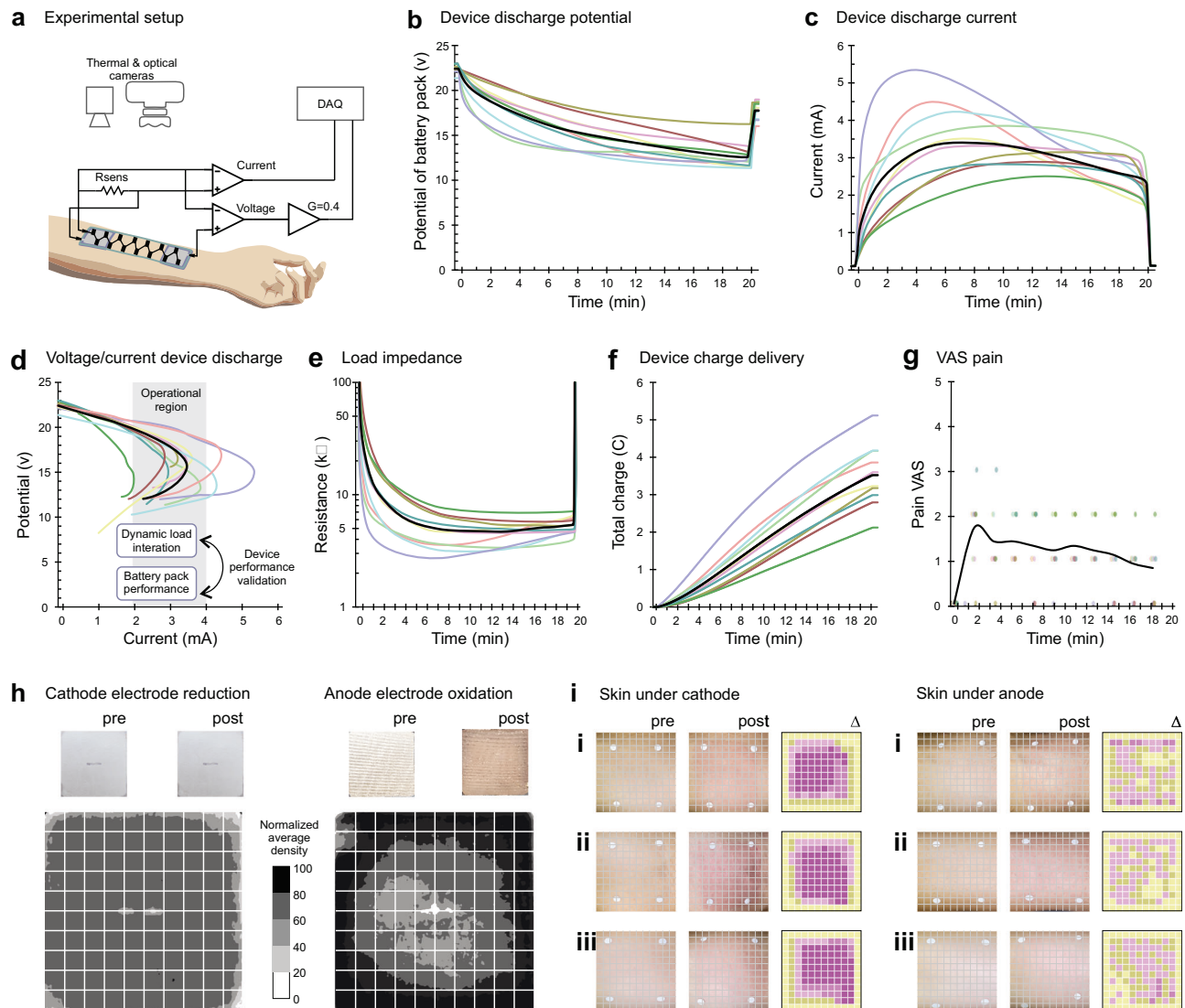
Fig. 5 | Validation of exemplary Wearable Disposable Electrotherapy self-limited discharge. a Experimental setup for the target application across subjects' forearms. Individual subjects (colored lines) and average (black) lines are shown. **b** Voltage of battery packs and (**c**) output current over 20 min of stimulation. **d** V-I curve of device throughout the stimulation. Compare these measured discharges with device-design simulation (Fig 5fii). **e** Impedance of the load (electrodes + skin), **f** cumulative charge delivered across the load, and **g** pain levels over the 20 min of stimulation. **h** Distribution of stimulation cathode electrode reduction and anode electrode oxidation. **i** Skin redness relative heat map under stimulation cathode electrode and under anode electrode, for three subjects (**i**, **ii**, **iii**). Subjects are indicated by the same color across panels.

tolerated (average pain VAS 1.1 ± 0.75; across 110 measurements never >3; Fig. 5g), with expected transient erythema and no lasting skin irritation. Subject's transient and mild perceptions of current flow (e.g., "tingling") are consistent with functional electrical delivery (i.e., activation of nerves[28]).

Uniformity of current delivery was assessed across electrodes and skin surfaces. Charge uniformity was imaged (pre/post discharge, 2D optical scan) at the anode stimulation electrode, as evidenced by corrosion, and at the cathode electrode, as evidenced by gas generation (Fig. 5h). Average normalized charge density was uniform at the cathode and moderately higher at electrode edges (annular) at the anode. Stimulation uniformity at the skin was assessed by high-resolution photography (pre/post discharge) of skin erythema (Fig. 5i; 29). Immediately post-discharge, erythema was relatively uniform under the cathode while milder and punctate under the anode. At appropriate doses, transient erythema is expected[29], non-hazardous and consistent with skin stimulation, and in the context of iontophoretic drug delivery and wound healing desired[5,28].

Functional conformability[23] is validated through the combination of impedance stability (Fig. 5e), current density uniformity (Fig. 5h, i), and tolerability (Fig. 5g). By achieving electronics-less design with device thickness of $400-700 \, \mu m$ thickness (Supplementary Fig. 2b), flexibility is governed by the design/layout of the battery pack, device thickness/flexural modulus, and device to skin surface ratio[30].

Applications of Wearable Disposable Electrotherapy platform

We demonstrate three applications of Wearable Disposable Electrotherapy by applying the described design framework (Fig. 2). For each application, the electrotherapy dose and mechanical consideration of application serves as the design input to the Wearable Disposable Electrotherapy analog and the validation of design outputs. The range of performance (design inputs) of these applications and the exemplary device are selected to demonstrate the platform's flexibility to broad electrotherapy applications. Current spans 2 orders of magnitude ($30 \, \mu A$ to $3 \, mA$), duration (~20 min to >2 hours) with $0.5-2 \, cm^2$ battery packs of 4–14 cells. Both homogeneous and inhomogeneous

battery pack sizing are demonstrated. Application-specific interfaces span 4.5 cm² to 25 cm² contacts, hydrogel or nonwoven sponge ion conductors, and varied stimulation anode/cathode materials (copper, zinc, silver, carbon and silver chloride). Battery packs and interfaces are packaged into application-specific enclosures (18 to 132 cm²), with mechanical design supporting conformability. Battery packs are designed to the targeted dose, accounting for application-specific loads by isotemporal-trajectory theory (Supplementary Notes 1).

Transcranial Direct Current Stimulation (tDCS) is a non-invasive brain stimulation technique[31], trialed for a range of neurological and psychiatric disorders[3,4]. A typical 'bi-frontal' dose is 1–4 mA (with 30 second ramp up/down), 20–30 min, ~25 cm² electrode on the EEG 10-10 F3/ F4 scalp positions. Bi-frontal Wearable Disposable Electrotherapy design inputs were with electrodes below hairline, using 2.5 ± 1 mA DC average to provide target electric field to the frontal cortex (max 2.3 V/m at the dorsolateral prefrontal cortex; Fig. 6a[32]) with ramp up $\tau > 30$ s and instantaneous peak current <3 mA. This design was based on load impedance under constant currents (1.5–4 mA; Fig. 6aiv). Integrated system design (Fig. 2) produced an articulated device architecture (Fig. 6ai) including 4 inhomogeneous cells (Fig. 6aii). Conformability is enhanced through the use of a single substrate over the interface (Supplementary Fig. 4biv) and bend-line cuts in the substrate, which facilitate deformation to the forehead (Supplementary Fig. 4bii). To deliver the prescribed dose, battery pack sizing (Eq. 2) resulted in an inhomogeneous configuration with 3 cells (1.6 cm²) with 34 wt% KOH electrolyte and 1 cell (1.4 cm²) with 0.7 wt% PAA polymer added to electrolyte that limits the peak current. The purpose of the PAA was to provide additional self-limited current through adaptive electrostatic and decreased ionic conductivity mechanisms (Supplementary Fig. 7; Supplementary Fig. 5g[33,34]). Designed devices were prototyped according to our manufacturing process (Supplementary Notes 2) and validated on human subjects (Fig. 6avii) demonstrating discharge performance within design specification and matching design theory (subject average current 2.35 ± 0.32 mA).

Iontophoresis is an established therapy passing DC through the skin for applications including hyperhidrosis and transdermal drug delivery[35]. A conventional iontophoretic dose uses ion-carrier nonwoven sponge interface (4 × 4 cm) with charge rated dose >30 mA-min (~1.8 C); when applied for 60 min sustaining an average current ~500 µA[36]. These served as the design inputs for the iontophoresis application Wearable Disposable Electrotherapy (Fig. 6b). System design (Fig. 2) yielded a Wearable Disposable Electrotherapy iontophoresis design (Fig. 6bii) using 4 homogeneous cells (2.0 cm2) with 0.7 wt% PAA polymer-supplemented electrolyte to self-limit the peak current. The conformability was enhanced by narrower substrate between two interfaces (Supplementary Fig. 4biii). Current flow simulation predicts resulting charge density of 31.2 µA/cm2 per second at the device-skin interface (Fig. 6bi). According to isotemporal trajectory theory (Supplementary Notes 1), the design was developed by measuring the load impedance under constant currents (200–700 µA; Fig. 6biv). The battery pack was accordingly sized and discharged (Fig. 6bv) and the iontophoresis-application Wearable Disposable Electrotherapy device built. Using a skin phantom, enhanced diffusion of ionic dye (molecular weight similar to the range of common drugs used in iontophoresis) was verified (Supplementary Fig. 8). Finally, devices were validated in human trials to produce the prescribed discharge performance: average charge 32.7 ± 11.60 mA-min in 60 min, with current 541 ± 193 µA (Fig. 7bvii).

Electrical stimulation can accelerate wound healing[34,37] Effective doses include low-intensity DC at 30–50 µA average over >2 hours. An integrated design process (Fig. 2) resulted in a wound healing-application Wearable Disposable Electrotherapy design including three battery cells, and stimulation electrode hydrogels on both sides of a wound dressing pad. The manufactured device is then placed on a skin adhesive for bandages. The substrate is made from a stretchable thermoplastic film with slots between each battery cell for additional flexibility (Fig. 6cii, Supplementary Fig. 4bii). During heat press sealing, the stretchable thermoplastic film undergoes copolymerization, eliminating the need for a separate adhesive layer between the two substrates. Using an interface device and a sourcemeter (10–50 µA), the load impedance was determined. Battery packs were sized according to isotemporal trajectory theory (Supplementary Notes 1) and the device was built accordingly. Current flow simulation predicted a resulting largely uniform current density through the targeted region (Fig. 6cii). Wearable Disposable Electrotherapy wound healing devices were then validated (Fig. 6cvii) demonstrating discharge performance within design inputs and matching design theory (average current 33 ± 12 µA).

Efficacy in accelerating wound healing was tested in a rodent full-thickness (6 mm diameter) excisional wounds model, applying stimulation using a tailored Wearable Disposable Electrotherapy device (300 ± 50 µA, 120 minutes daily for 14 days; Supplementary Fig. 9a). Bipolar stimulation hydrogels are positioned across wounds with nonwoven wound dressing over the wound (Supplementary Fig. 9b). Our form factor matches conventional bandages with hydrogels supporting functions of current delivery and adhesion over intact skin. Target current was verified (Supplementary Fig. 9f, g) with predicted current densities of ~0.6 A/m² produced across the wounds (FEM predicting target current densities; Supplementary Fig. 9c). Compared to sham bandages (no current), Wearable Disposable Electrotherapy significantly accelerated the rate of wound closure compared to the sham control, as evidenced by a significant interaction between treatment group and day of measurement ($\beta = -9.938$, SE = 3.887, t(121) = −2.557, $p = 0.012$; Group AB vs. Sham, spline interaction term).

Usability, economics, environmental, healthcare equity impact

Usability is a barrier to electrotherapy adoption, compliance, and effectiveness[11]. Conventional non-invasive devices require patients to be tethered to an electronic stimulator with numerous steps at and between each use. These obstacles complicate the treatment experience, throttle adoption, and impair compliance. Wearable Disposable Electrotherapy are thin, discreet, comfortable strips, with an application-specific single dose automatically delivered upon application to the skin (Figs. 5, 6). By fundamentally simplifying dissemination, storage, use, and disposal (Fig. 7), Wearable Disposable Electrotherapy usability is akin to pharmacotherapy or topical medication.

Wearable Disposable Electrotherapy economic efficiency is superior to traditional electrotherapy, which includes both durable electronics and consumables (batteries, disposable electrodes). Wearable Disposable Electrotherapy design is dematerialized for delivering a single dose (with minute quantities of electrochemically active materials; Supplementary Table 1). At the end of a treatment session, device materials are exhausted. In contrast, traditional devices: (1) Consume energy inefficiently (e.g., displays, voltage step-up) using stand-alone batteries (with inevitable waste); (2) Entail significant costs for materials, manufacturing (with higher Product Complexity Index), packaging, and shipment, amassing hundreds of grams of molded plastics, PCBs, electronics, and connections; moreover 3) This burden of durable equipment still requires disposable electrodes (~10 g per use including metal connectors; Supplementary Table 1). Wearable Disposable Electrotherapy prioritizes scalable manufacturing processes that are air-stable and less energy-intensive.

The production of electronics devices hinges on the utilization of rare earth elements and heavy metals, alongside manufacturing processes that are resource-intensive and detrimental to the environment (toxins and carbon emissions). The end-of-life disposal of electronics further compounds their environmental footprint. Wearable Disposable Electrotherapy production and use is inherently sustainable,
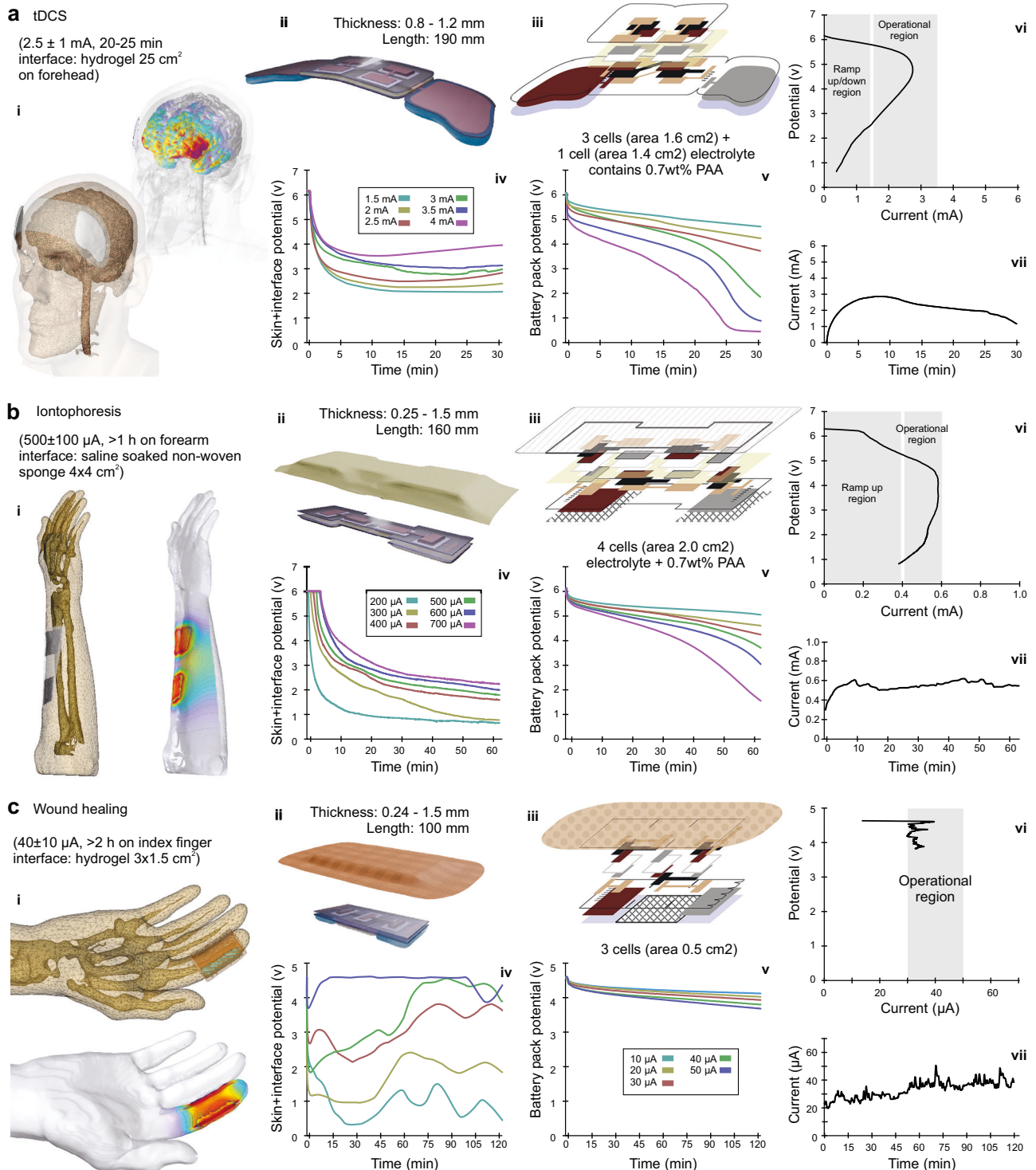
Fig. 6 | Application specific Wearable Disposable Electrotherapy design. The design pipeline validated for the exemplary device is applied to three use-cases: **a** tDCS, **b** iontophoresis, **c** accelerated wound healing - selected for efficacy supported by dozens of RCTs such that a Wearable Disposable Electrotherapy needs to reproduce the specified dose (design input). **i** High-resolution MRI-derived models simulate the desired tissue current delivery. **ii** The design process yields application-specific Wearable Disposable Electrotherapy devices, Thickness scaled 10x for clarity. **iii** Exploded device structure view. For each application battery sizing was modeled using Isotemporal Trajectory Theory using application-specific **iv** anatomical load and **v** cell galvanostatic tests (same color lines for matched current levels). **vi/vii** Validated device discharges are within specified application limits.

being dematerialized to essential components, using only abundant and environmentally benign materials (Supplementary Table 1), and additive manufacturing techniques (Supplementary Note 3) that avoid toxins.

Technology-centered health care advances (e.g., "smart" devices) often preferentially benefit users of privileged socioeconomic backgrounds. Wearable Disposable Electrotherapy has the potential to decrease healthcare inequity. Studies established traditional

a Wearable Disposable Electrotherapy: Distribution, use and disposal

Indication-specific distribution like pharmaceuticals or topical medicine.

Single dose, carried like a bandage, made from flexible printed materials.
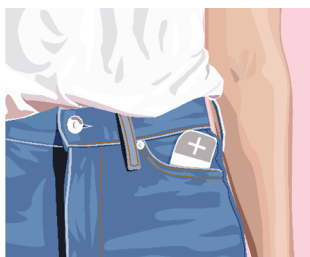
Single prescribed dose auto-initiated simply by placement.

Maximally dematerialized design, using environmentally-benign materials.

b Conventional Electrotherapy with durable equipment, batteries and disposable accessories: Distribution, use and disposal

Durable equipment, disposable accessories and batteries.

Carrying case for disconnected components.

Multi-step assembly and programming at each use, with subject tethered to equipment.

Packaging, accessories and electronic waste.
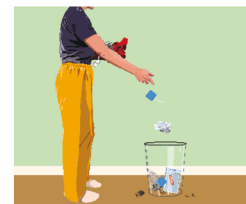
Fig. 7 | Wearable Disposable Electrotherapy eliminates barriers to use of traditional electrotherapy, and facilitates distribution akin to pharmacotherapy or topical medicine. Distribution, use and disposal of **a** Wearable Disposable Electrotherapy in comparison to **b** distribution, use and disposal of conventional electrotherapy. Distribution: Wearable Disposable Electrotherapy is dispensed in application-specific single-dose patches, similar to distribution of drugs or topical medicine. Carrying: Each Wearable Disposable Electrotherapy, containing a single dose, is like a bandage, while transporting conventional electrotherapy requires all components. Application: To use Wearable Disposable Electrotherapy, the patch is simply applied to skin - the device is discrete and automatically initiates and provides a single dose. With conventional electrotherapy a multi-step process involves tethering the electronic stimulator to the patient, using disposable electrodes, and programming/initiating therapy. Storage/disposal: The Wearable Disposable Electrotherapy minimizes environmental impact. Conventional electrotherapy devices have both durable electronics (whose eventual disposal includes toxic materials) and single-use accessories (which in themselves have more metal than a Wearable Disposable Electrotherapy).

electrotherapy as cost-effective healthcare, without discounting upfront equipment costs[37,38]. Conventional electrotherapies have a high startup cost (all durable equipment[39]) while Wearable Disposable Electrotherapy maintains the healthcare benefits without upfront equipment or training costs. The multi-step setup, programming, and maintenance of traditional electrotherapy is an accessibility barrier, while the auto-initiated bandage operation of Wearable Disposable Electrotherapy is intuitive[40] enhancing access to broader demographics. Deployability is a third factor for equitable access of medical devices, with Wearable Disposable Electrotherapy not requiring batteries/charging and can be simply distributed.

Discussion

In summary, we designed, fabricated, and validated the first electrotherapy platform using additive manufacturing with common environmentally-benign materials - without electronics. Device packaging, power, shape, and conformability design requirements are addressed using a specialized design workflow. Electrotherapy dose is "built-into" device architecture/chemistry, with discharge initiated simply by applying the device. We develop an associated theoretical framework for device design based on coupling between load and battery pack.

Although Wearable Disposable Electrotherapy is unique compared to all prior electrotherapy systems, there are limitations and opportunities. (1) Similar to how wound-specific adhesive bandages are tailored for specific body parts, new designs can be adapted to a range of shapes and anatomy. (2) Our scalable manufacturing can be integrated with advanced additive manufacturing techniques such as inkjet printing and pattern deposition[41,42]. (3) Such methods enhance precision in dose delivery by refining the spatial placement of active materials, enabling tight coupling between device configuration and therapeutic targets. (4) Clinical and human factors studies will assess usability, tolerability, and effectiveness. (5) Leveraging our platform for battery-to-load energy coupling, waveform modulation/adaptive dosing may be extended through integration of printable non-linear conductive elements[9,23] stretchable electronics/thin-film transistors[43] and printable sensor-like materials (e.g., sensitive to temperature, hydration, pressure). The theoretical framework and system architecture proven here establish a foundation for expanding Wearable Disposable Electrotherapy into a versatile platform for personalized, on-demand bioelectronic interventions.

Wearable Disposable Electrotherapy can be distributed like drugs or topical creams (Fig. 7), as dose/indication specific adhesive patch (Fig. 1a). A patient can carry a single device, simply apply it discreetly when needed, and then discard the device. Based on iontophoretic drug delivery, drug eluting patches are also thus made practical. The established principle of electrical wound healing can be made practical with disposable electrically driven bandages. Patches applied to the head can provide neuro-psychiatric therapies based on cranial nerve stimulation or cortex stimulation. This paper serves to show these and other applications are technically feasible.

Methods
Manufacture
Substrate preparation. The substrate is fabricated from 100 μm-thick PET sheets (McMaster #8567K44) which undergo a series of preparation steps: (1) Heat treating of the substrate for the purpose of mechanical stability by baking at 90 °C for 15 min; (2) Laser cutting to

perforate boundaries of the device and folding line as well as throughholes. This allows the pouch to be a part of the substrate sheet during printing steps, and subsequently to be separated for sealing of the battery pouch. The fold line facilitates accurate alignment of battery electrodes during folding while preventing easy tearing; (3) Washing with isopropyl alcohol followed by air drying; (4) Surface treatment with cold plasma (Relyon plasma piezo brush PZ3) to improve adhesion.

Printing of conductive tracks (interconnect, through holes, stimulation electrodes, current collectors). A copper conductive ink (Copprint LF-360) or silver conductive ink (Saral Silver 700) is screen printed (Novastar SPR-45 stencil/screen printer) onto both sides of the substrate (Supplementary Fig. 2a and c). Following printing[44], the substrate is heated in an oven (90 C) to facilitate the evaporation of the solvents present in the ink used. After baking, the thickness of the printed silver track is ~20 μm. Subsequently, a carbon passivation layer (Saral Carbon 700 A) is screen printed and baked in a similar fashion; this was only on the inner side with a screen template 1 mm wider than that used for silver from each side. After baking, the thickness of the printed carbon track is ~40 μm.

To establish an electrical connection between both sides of the substrate, we implement laser-cutting to create micrometer-sized holes in the form of an array in the substrate before printing. During the screen printing of the conductive inks on both sides of the substrate, the ink permeates these holes, creating a conductive path between the two sides of the substrate. The size and number of these holes are tailored to specific ink properties (rheology and particle size) to achieve reliable adhesion and conductivity. To support device verification and validation, three conductive tabs were added to the design at the battery pack terminals and at the cathode stimulation electrode, which allow monitoring of current and voltage.

Preparation of cathode ink, anode ink and electrolyte. The cathode ink used for exemplary device is composed of 70 wt% electrolytic manganese dioxide (EMD), 3.5 wt% carbon black as a conductive additive, 5 wt% KOH, 20 wt% deoxygenated DDI water, and 1.5 wt% PVA (average MW 94k) as a binder. The slurry is prepared by mixing water and PVA and KOH in a nitrogen box to prevent oxygen dissolution in water during mixing. The solution then is sealed and kept in the refrigerator at 4 °C. Prior to use, the mix of EMD powder and carbon black powder is added and mixed and then loaded into a syringe for application. The cathode ink for applications is composed of 79.5 wt% electrolytic manganese dioxide (EMD), 3.5 wt% carbon black as a conductive additive, 15.5 wt% deoxygenated DDI water, and 1.5 wt% SBR as a binder.

The anode ink used for exemplary device consists of 75 wt% zinc powder, 0.4 wt% zinc oxide as corrosion inhibitor, 5 wt% KOH, 17.8 wt% deoxygenated DDI water, 0.25 wt% PAA (average MW 450k), and 1.55 wt% Na-CMC (average MW 90k) as binders. The slurry is prepared by mixing all ingredients, except for zinc powder, in a nitrogen box to prevent oxygen dissolution. The slurry is then sealed and refrigerated at 4 °C. Prior to use, zinc powder is added to the solution inside of a syringe and mixed to create the anode ink. The anode ink for applications is composed of 74 wt% zinc powder, 0.3 wt% zinc oxide as corrosion inhibitor, 23.5 wt% deoxygenated DDI water, 1.4 wt% Na-CMC as filler, and 0.8 wt% SBR as binder.

The electrolyte is formulated with 66 wt% deoxygenated DDI water and 34 wt% KOH.

Sealing method. The device is sealed using a double-sided acrylic adhesive designed for low surface energy plastics, with an interior carrier film for enhanced mechanical stability with a thickness (0.17 mm) less than the battery pack cells and interconnects (3 M 9495LE). The double-sided adhesive sheet is cut (prior to removing the liner of both

sides) using a laser cutter into two strips, each with openings corresponding to cells on one row of the battery pack (Supplementary Fig. 3f). When placed on the substrate a gap between the two adhesive strips forms the central channel of the venting system (Supplementary Fig. 2d and 3f).

Placement of separator. The separator membrane (Celgard 5550) used consists of polypropylene film laminated to a polypropylene nonwoven fabric, coated with hydrophilic surfactant for aqueous applications. This membrane has a thickness of 110 μm and 55% porosity, for high electrolyte retention and ion conductivity for high discharge rate. The membrane is laser cut to appropriate size and placed on the cell using cut double sided tape.

Vent channel and valves. After placing the membranes on double sided tape, thin strips are printed on the adhesive using non-stick ink (1 mm width), connecting the middle of the battery cell to the vent channel (Supplementary Figs. 2d and 3c). These thin strips mask the adhesive, creating normally closed valves, they provide an escape for air (during battery pack sealing) or generated hydrogen by the cells, to the vent channel.

Printing of active materials on current collectors. In the exemplary device each membrane is saturated with 9.5 mg (8 μL) of electrolyte before printing active materials. The volume of electrolyte is crucial to control since insufficient electrolyte reduces battery performance, while excess electrolyte wets the surface of double-sided tape resulting in poor sealing. Then anode and cathode inks are deposited on printed substrates using a screen/stencil. Immediately after printing anode ink, double sided tapes with soaked membranes are placed on two anode rows of the device. This prevents printed zinc from drying. By folding the device on its fold line, both sides of the substrate meet in alignment to form a sealed battery pack (Supplementary Fig. 2a). The sealed battery pack goes through a roller from each side to the middle of the device where the vent channel is to push trapped air out of cells through valves.

Battery pack quality control. After compressing the pack, terminals of the pack are connected to a multimeter to read the initial open circuit voltage (IOCV). Some manufacturing problems can be detected by observing subtle changes of voltage.

Interface hydrogel application. Ion conductive hydrogels (Axelgaard AG625) are cut to the size (45 mm×56 mm, 25.2 cm²) and placed on the stimulation electrodes. As needed, fastening (non-conductive) hydrogel (Axelgaard AG535) can be used in between stimulation electrodes. The hydrogels are covered with PET liner until use. The hydrogel placement step was omitted for battery pack discharge verification tests. The optimization of hydrogel (and associated stimulation electrode material) for the exemplary application followed protocols developed in our lab[18,22,23,45] screening for (a) tolerability; (b) skin irritation; (c) impedance (compliance voltage); and (d) material/mechanical properties.

Device verification

Electrical performance verification of cell/battery packs under constant current discharge was conducted using a sourcemeter (Keithley 2450 SMU). Electrochemical impedance spectroscopy (EIS) experiments were conducted with a Prinston Applied VersaSTAT 4 Potentiostat/Galvanostat. AC impedance measurements were performed potentiostatically at open circuit voltage and a small signal stimulus of 5 mV within a frequency range of 10 mHz–10 kHz. The test is conducted with 60 data points distributed across the frequency range on a logarithmic scale. The battery model components were selected based on comparable electrochemistry analysis[26] and fit to EIS data (AMETEK,

ZView). Model parameters reflect mass transfer, chemical kinetics, and electrical resistance of current collectors and conductive additives in electrodes, from which device chemistry (particle size, electrode porosity) and structure (thickness of electrode, compaction) can be refined. This includes the upper limit on current density limited by mass transfer of charge carriers. SEM images recorded using SUPRA 55, with an acceleration voltage of 16 kV and backscattered electron detector.

Load characterization and validation

Participants. The study was conducted following protocols and procedures approved by the Institutional Review Board of the City College of New York. A total of 30 volunteer participants (17 male, 13 female) between the ages of 19 and 76 years (M = 31.2, SD = ±12.6) were enrolled in the study. Participants self-identified as Middle Eastern ($n = 9$), Asian ($n = 9$), White ($n = 8$), and Hispanic ($n = 4$). Subjects were recruited through local advertisements and provided written informed consent prior to participation. Participants received financial compensation for their involvement in the research.

Screening and exclusion criteria. Participants were excluded if they presented with any skin disorder at or near stimulation locations that compromised skin integrity, such as eczema, rashes, blisters, open wounds, burns including sunburns, cuts, or other skin defects, as the goal of this study was not to determine if skin impairments influence the tolerability or to access electrical stimulation to enhance wound healing.

Stimulation was applied to the ventral or dorsal side of the subject's left or right forearm. No more than one dose was applied to a region per day (e.g., ventral surface of right arm). All devices were at room temperature (22 °C) immediately prior to testing.

Load characterization. For load characterization tests, devices with the same design as Wearable Disposable Electrotherapy but with only interface components and without deposition of active materials were made. Prior to the test, subjects' forearms were cleansed with soap and water and then dried. After placement of ion conductive hydrogels, the monitoring tabs were connected to a sourcemeter (Keithley 2450 SMU). According to the test, the sourcemeter output was set to either constant voltage with a peak current limit, or to constant current with a voltage compliance limit. Output was enabled before placement of the test device on skin.

Temperature was recorded using three thermocouple probes placed in the empty battery pouch, one over the anode stimulation electrode, one over the cathode stimulation electrode and one in the middle of the device over fastening hydrogel. Photographs were taken immediately before and after stimulation under consistent lighting conditions and skin temperature was recorded using a thermal camera (FLIR One Pro). At the beginning and during stimulation, subjects reported subjective pain on a VAS scale every 2 min. Approximately 24 hours after stimulation, subjects' skin was evaluated for any enduring skin irritation.

Validation. The procedure was similar to load tests using the interface test device; instead of connecting the device to the sourcemeter, the Wearable Disposable Electrotherapy Device with active batteries was used. To record the voltage and current of the device, a custom high impedance analog interface was used (0.4 attention factor), a 100 Ω series resistor (for current), and acquisition system (DATAQ DI-1100).

Graphics. Graphics and elements were created using CorelDRAW Graphics Suite 2015 (Corel Corp., ON, CA), Blender 2019 (Blender Foundation), SolidWorks 2022 (Dassault Systemes Corp., MA, USA), or Adobe Illustrator 2019 (Adobe Inc., CA, USA).

In vivo rat wound-healing model

All animal procedures were approved by the Institutional Animal Care and Use Committee (IACUC) at The City College of New York (CCNY) (protocol #2024-0003) and conducted in compliance with the approved guidelines. Male Sprague-Dawley (SD) rats (Charles River Laboratories) aged 7–9 weeks (250–350 g) were acclimated to the facility for at least four days prior to surgery[46]. Under isoflurane anesthesia, the dorsal fur was removed by shaving and depilation, and two full-thickness circular excisional wounds (6 mm diameter) were created on the dorsum using a biopsy punch. Load characterization and device output verification followed procedure from human experiments.

For in-vivo wound-healing tests, stimulation devices (Supplementary Fig. 9) were designed according to our pipeline (Fig. 2) and calibrated using isotemporal trajectory theory (Supplementary Notes 1) to deliver current of $300 \pm 50\ \mu A$[47] for 120 minutes. The device included non-woven PET wound dressing (30 mm × 15 mm) with a silicone wound contact layer, positioned over the wound. On both sides of the wound dressing, two stimulation electrodes (30 mm×15 mm) are placed. These devices were positioned bilaterally across the wound, adhered to the skin using the hydrogels, and further secured with jackets. Daily stimulation conditions were either (groups): (a) Wearable Disposable Electrotherapy with 300 μA target dose for 120 minutes ($n = 4$); (b) Control rats ($n = 3$) which underwent the same procedures[48] but without electrical stimulation; c) Stimulation with electronics-based device (sourcemeter) at 300 μA constant current for 120 minutes. Images were captured using an AmScope MU300 camera installed on microscope eyepiece while rats were under isoflurane anesthesia. Wound areas were quantified using MATLAB and ImageJ. Open wounds were scored based on the red intensity compared to the surrounding skin and newly formed tissue[49]. Stimulation (on control bandages) was applied daily and wounds monitored for 14 days, starting from the day of surgery[50].

FEM Device Stimulation

For the exemplary device, we developed a computer-aided design (CAD) model of the Wearable Disposable Electrotherapy prototype and underlying superficial tissue. The biophysical and thermo-electrical properties of biological tissues were based on previous studies and heat-transfer biophysics followed standard assumptions and methods[51,52]. An approximate temperature distribution throughout a perfused tissue was predicted using Pennes bio-heat transfer equation(46)[52]. For the thermal boundary conditions, all external boundaries were insulated except the top surface which was assigned heat flux. For the tDCS device, we used our previously detailed[53] and verified[54] MRI-derived (1 mm³ T1/T2; 36-year-old male) head model. For the iontophoresis device model and the wound healing device model, a forearm/hand model was developed from a high-resolution MRI (1.25 mm³ T1/T2/Petra; 33-year-old male). For the rat wound healing device model, an MRI-derived (0.35 mm³ T1/T2/Petra; adult male SD) high-resolution rat model was developed. Two 6 mm diameter regions were segmented in the superficial skin layer to mimic the experimental wound.

CAD structures (devices) were modeled in SolidWorks 2022 (Dassault Systemes Corp., MA, USA) and Simpleware ScanIP (Synopsys, WA, USA) imported and numerically solved in COMSOL Multiphysics 5.6 (COMSOL Multiphysics, Boston, MA) under conventional parameters and quasi-static electromagnetics[55,56]. The resulting finite element model comprised >32 M tetrahedral elements (>11 M degrees of freedom) for the exemplary device, >2 M tetrahedral elements (>2 M degrees of freedom) for tDCS model, >50 M tetrahedral elements (>72 M degrees of freedom) for the iontophoresis model, >35 M tetrahedral elements (>54 M degrees of freedom) for the wound healing model, and > 5 M tetrahedral elements (>7 M degrees of freedom) for the rat wound healing model.

Statistical analysis

A linear mixed-effect model fitted using restricted maximum likelihood estimation was used to evaluate the effects of treatment group, day, and their interaction on the relative change in wound healing. Critical value of <0.05 was accepted as a statistical difference between groups. Each data point comes from a distinct sample.

Ethics

Every experiment involving animals, human participants, or clinical samples has been carried out following a protocol approved by an ethical commission. Each participant gave informed written consent.

Reporting summary

Further information on research design is available in the Nature Portfolio Reporting Summary linked to this article.

Data availability

Source data are provided with this paper.

Code availability

No code was developed for this project.

References

1. Vance, C. G. T. et al. Using TENS for pain control: the state of the evidence. *Pain. Manag.* **4**, 197–209 (2014).
2. Coppola, G. et al. Neuromodulation for chronic daily headache. *Curr. Pain. Headache Rep.* **26**, 267–278 (2022).
3. Fregni, F. et al. Evidence-based guidelines and secondary meta-analysis for the use of transcranial direct current stimulation in neurological and psychiatric disorders. *Int. J. Neuropsychopharmacol.* **24**, 256–313 (2021).
4. Antal, A. et al. Low intensity transcranial electric stimulation: safety, ethical, legal regulatory and application guidelines. *Clin. Neurophysiol.* **128**, 1774–1809 (2017).
5. Thakral, G. et al. Electrical stimulation to accelerate wound healing. *Diabet. Foot Ankle* **4**, 22081 (2013).
6. Jiang, Y. et al. Wireless, closed-loop, smart bandage with integrated sensors and stimulators for advanced wound care and accelerated healing. *Nat. Biotechnol.* **41**, 652–662 (2023).
7. Bikson, M. et al. Limited output transcranial electrical stimulation 2023 (LOTES-2023): updates on engineering principles, regulatory statutes, and industry standards for wellness, over-the-counter, or prescription devices with low risk. *Brain Stimul.* **16**, 840–853 (2023).
8. Karpiński, T. M. Selected medicines used in iontophoresis. *Pharmaceutics* **10**, 204 (2018).
9. Wang, W. et al. Neuromorphic sensorimotor loop embodied by monolithically integrated, low-voltage, soft e-skin. *Science* **380**, 735–742 (2023).
10. Jiang, M. et al. Advances in smart sensing and medical electronics by self-powered sensors based on triboelectric nanogenerators. *Micromachines* **12**, 698 (2021).
11. Guleyupoglu, B. et al. Classification of methods in transcranial electrical stimulation (tES) and evolving strategy from historical approaches to contemporary innovations. *J. Neurosci. Methods* **219**, 297–311 (2013).
12. Dhote, V. et al. Iontophoresis: a potential emergence of a transdermal drug delivery system. *Sci. Pharm.* **80**, 1–10 (2011).
13. Peebles, I. S., Phillips, T. O. & Hamilton, R. H. Toward more diverse, inclusive, and equitable neuromodulation. *Brain Stimul.* **16**, 737–741 (2023).
14. Ye, C. et al. A wearable aptamer nanobiosensor for non-invasive female hormone monitoring. *Nat. Nanotechnol.* **19**, 330–337 (2024).
15. Xu, G. et al. Battery-free and wireless smart wound dressing for wound infection monitoring and electrically controlled on-demand drug delivery. *Adv. Funct. Mater.* **31**, 2100852 (2021).
16. Peterchev, A. V. et al. Fundamentals of transcranial electric and magnetic stimulation dose: definition, selection, and reporting practices. *Brain Stimul.* **5**, 435–453 (2012).
17. Merrill, D. R., Bikson, M. & Jefferys, J. G. R. Electrical stimulation of excitable tissue: design of efficacious and safe protocols. *J. Neurosci. Methods* **141**, 171–198 (2005).
18. Minhas, P. et al. Electrodes for high-definition transcutaneous DC stimulation for applications in drug delivery and electrotherapy, including tDCS. *J. Neurosci. Methods* **190**, 188–197 (2010).
19. Gaikwad, A. M. et al. A flexible high potential printed battery for powering printed electronics. *Appl. Phys. Lett.* **102**, 233303 (2013).
20. Newman, J. S. & Tobias, C. W. Theoretical analysis of current distribution in porous electrodes. *J. Electrochem. Soc.* **109**, 1183–1191 (1962).
21. Lanzi, O. & Landau, U. Effect of pore structure on current and potential distributions in a porous electrode. *J. Electrochem. Soc.* **137**, 585–591 (1990).
22. Paneri, B. et al. Tolerability of repeated application of transcranial electrical stimulation with limited outputs to healthy subjects. *Brain Stimul.* **9**, 740–754 (2016).
23. Khadka, N. et al. Dry tDCS: tolerability of a novel multilayer hydrogel composite non-adhesive electrode for transcranial direct current stimulation. *Brain Stimul.* **11**, 1044–1053 (2018).
24. Bora, D. J. & Dasgupta, R. Estimation of skin impedance models with experimental data and a proposed model for human skin impedance. *IET Syst. Biol.* **14**, 230–240 (2020).
25. Unal, G. et al. Quasi-static pipeline in electroconvulsive therapy computational modeling. *Brain Stimul.* **16**, 607–618 (2023).
26. Lazanas, A. C. & Prodromidis, M. I. Electrochemical impedance spectroscopy—a tutorial. *ACS Meas. Sci. Au* **3**, 162–193 (2023).
27. Khadka, N. et al. Minimal heating at the skin surface during transcranial direct current stimulation. *Neuromodulation* **21**, 334–339 (2018).
28. Xu, X. et al. Effects of electrical stimulation on skin surface. *Acta Mech. Sin.* **37**, 1–29 (2021).
29. Ezquerro, F. et al. The influence of skin redness on blinding in transcranial direct current stimulation studies: a crossover trial. *Neuromodulation* **20**, 248–255 (2017).
30. Liu, S. et al. Conformability of flexible sheets on spherical surfaces. *Sci. Adv.* **9**, eadf2709 (2023).
31. Woods, A. J. et al. A technical guide to tDCS, and related non-invasive brain stimulation tools. *Clin. Neurophysiol.* **127**, 1031–1048 (2016).
32. Seibt, O. et al. The pursuit of DLPFC: non-neuronavigated methods to target the left dorsolateral pre-frontal cortex with symmetric bicephalic transcranial direct current stimulation (tDCS). *Brain Stimul.* **8**, 590–602 (2015).
33. Tran, T. N. T. et al. Effects of crosslinker concentration in poly(acrylic acid)-KOH gel electrolyte on performance of zinc-air batteries. *Batteries Supercaps* **3**, 409–416 (2020).
34. Lützenkirchen, J. et al. Comparison of various models to describe the charge-pH dependence of poly(acrylic acid). *J. Chem. Eng. Data* **56**, 1602–1612 (2011).
35. Dixit, N. et al. Iontophoresis-an approach for controlled drug delivery: a review. *Curr. Drug Deliv.* **4**, 1–10 (2007).
36. Anderson, C. R. et al. Effects of iontophoresis current magnitude and duration on dexamethasone deposition and localized drug retention. *Phys. Ther.* **83**, 161–170 (2003).
37. Hao, Q., Horton, J. & Hamson, A. Electrostimulation devices for wounds. *Can. J. Health Technol.* **3**, 7 (2023).
38. Simpson, K. N. et al. Cost-effectiveness of transcranial magnetic stimulation in the treatment of major depression: a health economics analysis. *Adv. Ther.* **26**, 346–358 (2009).
39. Leiphart, J. et al. Economic inequities in the application of neuromodulation devices. *Cureus* **11**, eXXXX (2019).

40. Kadakia, K. T. et al. Challenges and solutions to advancing health equity with medical devices. *Nat. Biotechnol.* **41**, 607–609 (2023).

41. Kang, J. S. et al. Inkjet printed electronics using copper nanoparticle ink. *J. Mater. Sci. Mater. Electron.* **21**, 1213–1220 (2010).

42. Driscoll, N. et al. MXene-infused bioelectronic interfaces for multi-scale electrophysiology and stimulation. *Sci. Transl. Med.* **13**, eabf8629 (2021).

43. Cantarella, G. et al. Buckled thin-film transistors and circuits on soft elastomers for stretchable electronics. *ACS Appl. Mater. Interfaces* **9**, 28750–28757 (2017).

44. Sousa, R. E., Costa, C. M. & Lanceros-Méndez, S. Advances and future challenges in printed batteries. *ChemSusChem* **8**, 3539–3555 (2015).

45. Guleyupoglu, B. et al. Reduced discomfort during high-definition transcutaneous stimulation using 6% benzocaine. *Front. Neuroeng.* **7**, 28 (2014).

46. Masson-Meyers, D. S. et al. Experimental models and methods for cutaneous wound healing assessment. *Int. J. Exp. Pathol.* **101**, 21–37 (2020).

47. Rabbani, M. et al. Making sense of electrical stimulation: a meta-analysis for wound healing. *Ann. Biomed. Eng.* **52**, 153–177 (2024).

48. Kaveti, R. et al. Water-powered, electronics-free dressings that electrically stimulate wounds for rapid wound closure. *Sci. Adv.* **10**, eado7538 (2024).

49. Grey, J. E., Enoch, S. & Harding, K. G. Wound assessment. *BMJ* **332**, 285–288 (2006).

50. Song, J. W. et al. Bioresorbable, wireless, and battery-free system for electrotherapy and impedance sensing at wound sites. *Sci. Adv.* **9**, eade4687 (2023).

51. Zannou, A. L., Khadka, N. & Bikson, M. Bioheat model of spinal column heating during high-density spinal cord stimulation. *Neuromodulation* **26**, 1362–1370 (2023).

52. Datta, A., Elwassif, M. & Bikson, M. Bio-heat transfer model of transcranial DC stimulation: comparison of conventional pad versus ring electrode. *Conf. Proc. IEEE Eng. Med. Biol. Soc.* **2009**, 670–673 (2009).

53. Datta, A. et al. Inter-individual variation during transcranial direct current stimulation and normalization of dose using MRI-derived computational models. *Front. Psychiatry* **3**, 91 (2012).

54. Huang, Y. et al. Measurements and models of electric fields in the in vivo human brain during transcranial electric stimulation. *eLife* **6**, e18834 (2017).

55. Wang, B. et al. Quasistatic approximation in neuromodulation. *J. Neural Eng.* **21**, 041002 (2024).

56. Bikson, M. et al. Modeling sequence and quasi-uniform assumption in computational neurostimulation. *Prog. Brain Res.* **222**, 1–23 (2015).

Acknowledgements

Author contributions

M.B., A.C., and M.FR. conceived the idea. K.D. designed and performed human trials. M.B.K. designed and performed animal tests. M.B.K., N.K., Z.C., and O.V. designed and performed modeling. R.B., B.B., M.S., T.L., M.R.D.U., M.Z., K.S., A.R., and M.T. designed or performed bench experiments. All authors contributed to drafting the manuscript and gave approval to the final version of the manuscript.

Competing interests

The City University of New York holds patents on brain stimulation or battery technology with MB, AC, MFR as inventor, including a patent application on printed battery-powered electrotherapy (application # USPTO 18/955,575, PCT/US24/56942). MB has equity in Soterix Medical Inc., an electrotherapy company. AC has equity in Urban Electric Power, a battery company. MB consults, received grants, assigned inventions, and served on the SAB of SafeToddles, Boston Scientific, GlaxoSmithKline, Biovisics, Mecta, Lumenis, Halo Neuroscience, Google-X, i-Lumen, Humm, Allergan (AbbVie), Apple, Ybrain, Ceragem, RemZ, some are electrotherapy companies. The authors declare no other competing interests.

Additional information

Supplementary information The online version contains supplementary material available at https://doi.org/10.1038/s41467-025-64101-x.

Correspondence and requests for materials should be addressed to Mohamad FallahRad.

Peer review information *Nature Communications* thanks the anonymous reviewers for their contribution to the peer review of this work. A peer review file is available.

Reprints and permissions information is available at http://www.nature.com/reprints

Publisher's note Springer Nature remains neutral with regard to jurisdictional claims in published maps and institutional affiliations.